Dynamic Analysis of a Cable-Stayed Concrete-Filled Steel Tube Arch Bridge under Vehicle Loading

Wei Wang[1]; Wangchen Yan[2]; Lu Deng, Ph.D., M.ASCE[3]; and Houjun Kang, Ph.D.[4]

Abstract: This paper presents the results from a dynamic analysis of a cable-stayed concrete-filled steel tube arch bridge under vehicle loading. The study is carried out based on a three-dimensional vehicle-bridge coupled model. A finite-element model for the bridge is first developed and validated based on field measurement data. A truck specified by industry standards is adopted for vehicle loading in the analysis and is simulated as a multidegree-of-freedom vehicle model. Three important indexes, including the dynamic impact factor, perceptible level of vibration, and ride comfort of the bridge, are investigated. A parametric study is conducted to investigate the effects of a few important parameters, including the vehicle loading condition, vehicle speed, and road surface condition, on the three indexes. Results from the analysis show the following: (1) the dynamic impact factors, which vary between different bridge components/locations, are significantly affected by the three parameters; the impact factors of key structural components of the bridge studied are generally below the value of 0.33 specified in previous design specifications; (2) the perceptible level of bridge vibration is greatly affected by the road surface condition and vehicle loading condition; pedestrians can feel it to be slightly hard to walk on the bridge when two trucks move side by side under poor road surface conditions; and (3) the ride comfort of the bridge decreases as the road surface condition becomes worse, and drivers can feel a little uncomfortable under poor road surface conditions. Because all three indexes studied are found to be greatly affected by the road surface condition, establishing and maintaining a regular program of maintenance is very important to assure both the safety and serviceability of the bridge studied. **DOI: 10.1061/(ASCE)BE.1943-5592.0000675.** © *2014 American Society of Civil Engineers.*

Author keywords: Dynamic analysis; Cable-stayed concrete-filled steel tubular (CFST) arch bridge; Dynamic impact factor; Perceptible level of vibration; Ride comfort.

Introduction

In recent years, concrete-filled steel tubular (CFST) arch bridges have attracted much attention and have been rapidly developing in some countries, such as China and Japan (Han et al. 2001; Wu et al. 2006). The CFST arch bridges can fully use the advantages of both concrete and steel materials, which, in turn, reduce the construction cost. Nevertheless, the span length of arch bridges is still limited because of stability problems with increasing arch spans.

To strive for larger span lengths for arch bridges, much effort has been devoted to developing new hybrid bridges in recent years. A new type of cable-supported bridge, namely, a cable-stayed concrete-filled steel tube arch bridge, was proposed (Klein and Yamout 2003; Nakamura et al. 2009). This bridge concept uses both stay cables and arches to support the bridge deck, and it exhibits superior mechanical behaviors compared with conventional arch bridges in terms of the stability of arch ribs (Nakamura et al. 2009). The first cable-stayed CFST arch bridge was constructed in Kuala Lumpur, Malaysia, in 2002. Five years later, the first cable-stayed CFST arch bridge in China, Liancheng Bridge, was opened to traffic (Luo et al. 2005). This bridge is different from the early cable-stayed CFST arch bridges proposed in the literature and the first cable-stayed CFST arch bridge built in Malaysia in that the stay cables of the Liancheng Bridge are anchored on the arch ribs instead of the bridge deck.

Fully understanding the static and dynamic behaviors of a new bridge concept is crucial when evaluating the bridge concept. The static behavior of the Liancheng Bridge has been investigated in depth, both analytically and experimentally, by Kang et al. (2013). Simple modal analysis of this new bridge concept has also been conducted by some researchers (Luo et al. 2005; Zhao et al. 2005). However, a full dynamic analysis of the Liancheng Bridge and this type of cable-stayed CFST arch bridge under vehicle loading has not yet been conducted. Therefore, it is meaningful to evaluate the dynamic responses of the bridge under vehicle loading for further development and evaluation of this type of bridge.

In this paper, a finite-element model for the Liancheng Bridge is first developed and validated using field measurement data. Then, a three-dimensional vehicle-bridge coupled model is used to analyze the dynamic responses of the Liancheng Bridge under vehicle loading. The two main purposes of this paper are to (1) investigate the dynamic impact behavior of the cable-stayed CFST arch bridge in terms of the impact factor (IM) of critical bridge components, and (2) evaluate the perceptible level of vibration and ride comfort of the cable-stayed CFST arch bridge. The authors hope that the results from this study can shed light on some issues that need to be considered in the practical design of this type of bridge.

Brief Description of the Liancheng Bridge

The Liancheng Bridge, also called the Fourth Xiangjiang River Bridge, links the east and west of Xiangtan (a city in Hunan

[1]Graduate Student, College of Civil Engineering, Hunan Univ., Changsha, Hunan 410082, China. E-mail: jswnww@hnu.edu.cn

[2]Graduate Student, College of Civil Engineering, Hunan Univ., Changsha, Hunan 410082, China. E-mail: ywchen92@163.com

[3]Professor, College of Civil Engineering, Hunan Univ., Changsha, Hunan 410082, China (corresponding author). E-mail: denglu@hnu.edu.cn

[4]Associate Professor, College of Civil Engineering, Hunan Univ., Changsha, Hunan 410082, China. E-mail: khjun@hnu.edu.cn

Note. This manuscript was submitted on March 18, 2014; approved on July 7, 2014; published online on July 31, 2014. Discussion period open until December 31, 2014; separate discussions must be submitted for individual papers. This paper is part of the ***Journal of Bridge Engineering***, © ASCE, ISSN 1084-0702/04014082(12)/$25.00.

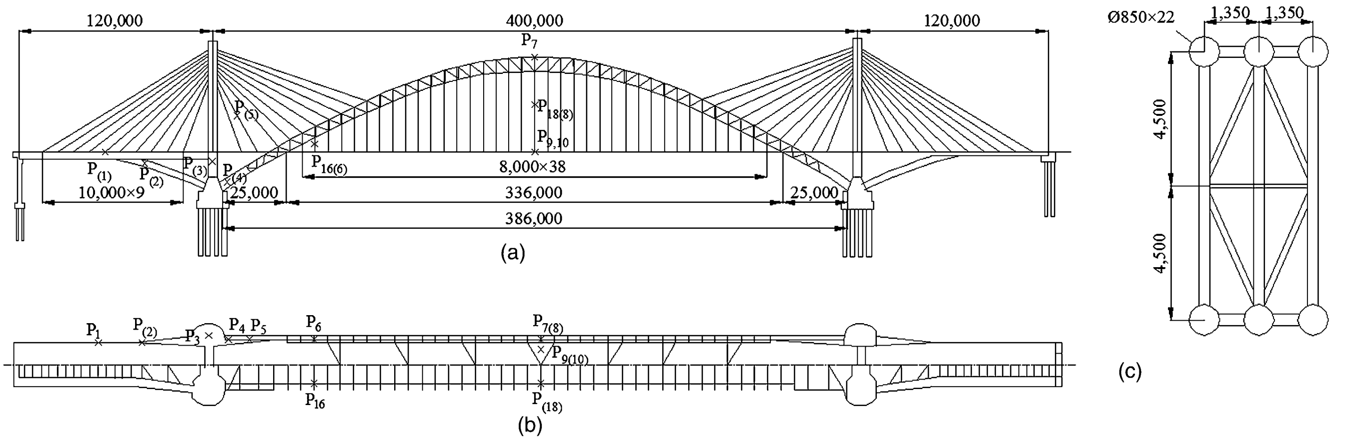

Fig. 1. General view of the Liancheng Bridge (in millimeters): (a) elevation view; (b) plan view; (c) cross section of main arch rib

Province, China), which is divided into two parts by the Xiangjiang River. As shown in Fig. 1(a), this cable-stayed CFST arch bridge has a unique configuration, which combines the features of an arch bridge and a two-pylon cable-stayed bridge. The main span of the bridge is 400 m in length, and the side spans are 120 m in length. The bridge is 27 m in width. The bridge has two parallel arch ribs, each of which has a rectangle cross section consisting of six steel tubes, as shown in Fig. 1(c). The six steel tubes have an outer diameter of 850 mm and a thickness that varies between 20 and 28 mm depending on the position of the arch rib. The main arch floor system, supported by two rows of 39 steel wire rope hangers with intervals of 8 m, is composed of the deck, I-shaped transverse girders, and longitudinal stringers. The stay cables are anchored on the bridge deck and arch ribs with intervals of 10 and 8 m, respectively.

The basic material properties of the main structural components of the Liancheng Bridge, including the cross-sectional area, A, and elastic modulus, E, are given in Table 1. In this study, it was assumed that (1) the geometric nonlinearity is not considered when evaluating the bridge responses under vehicle loading, (2) the stress-strain relationships of steel and concrete are both linear, and (3) the deformation of the steel tube is equal to that of the concrete inside along the boundary of the two materials, and, consequently, slip between the steel tube and filled concrete will not occur (Yoshimura et al. 2006).

Table 1. Cross-Sectional Area (A) and Elastic Modulus (E) of Important Structural Components of Liancheng Bridge

Content	A (m^2)	E (N/m^2)
Main arch rib (steel tube only)	1.430×10^{-3} (upper rib)	2.1×10^{11}
Bracing	1.304×10^{-3} (lower rib)	2.1×10^{11}
Hanger	4.128×10^{-3}	2.1×10^{11}
Cross girder	2.117×10^{-3}	2.05×10^{11}
Stay cable	8.000×10^{-1}	2.1×10^{11}
Main tower	4.340×10^{-3}	1.95×10^{11}
Arch rib of side span	1.143×10^{1} (upper tower)	3.5×10^{10}
	1.074×10^{1} (middle tower)	3.5×10^{10}
	1.304×10^{1} (lower tower)	3.5×10^{10}
	8.800×10^{0}	3.5×10^{10}

Bridge Model

Based on the design drawings, a three-dimensional finite-element model of the bridge was developed using the *ANSYS 10.0* program as shown in Fig. 2. The arch ribs, K-shaped bracings, main towers, and side-span systems were modeled by three-dimensional beam elements (Beam44). The stay cables and hangers were modeled using three-dimensional link elements (Link10). The main bridge deck and transverse girders were modeled using three-dimensional solid elements (Solid45). For the boundary conditions, both ends of the main arch ribs, main towers, and arch ribs of the side spans were fixed in all degrees of freedom; translational movements of the ends of the two side spans in all three directions were fixed, whereas rotation along the lateral axis was allowed.

A modal analysis was performed on the finite-element model of the Liancheng Bridge, and the natural frequencies and corresponding mode shapes of the first 10 vibration modes are provided in Table 2 and Fig. 3, respectively. The first free vibration mode, with a frequency of 0.238 Hz, corresponds to the first symmetrical lateral vibration mode, whereas the first vertical vibration mode (fourth mode overall), an asymmetrical mode, has a frequency of 0.482 Hz.

The natural frequencies obtained from the bridge model were compared with the best available data (Luo et al. 2005) as shown in Table 2. The differences between the two sets of results are all within 10%, except for the fourth vibration mode, which demonstrates the reliability of the developed finite-element model.

Vehicle Model

The vehicle used in the current study is the HS20-44 truck adopted in AASHTO's *LRFD Bridge Design Specifications* (AASHTO 2004). The vehicle is simulated as a multidegree-of-freedom model consisting of 11 independent degrees of freedom (Huang and Wang 1992; Shi et al. 2008; Deng and Cai 2010a, b). The analytical truck model is illustrated in Fig. 4. Detailed properties for the HS20-44 truck model, including the geometry, mass distribution, damping, and stiffness of the tires and suspension systems, can be found in the literature (Shi 2006; Deng and Cai 2010a).

Vehicle-Bridge Coupled System

Equation of Motion of the Vehicle

The equation of motion for a vehicle can be expressed as follows:

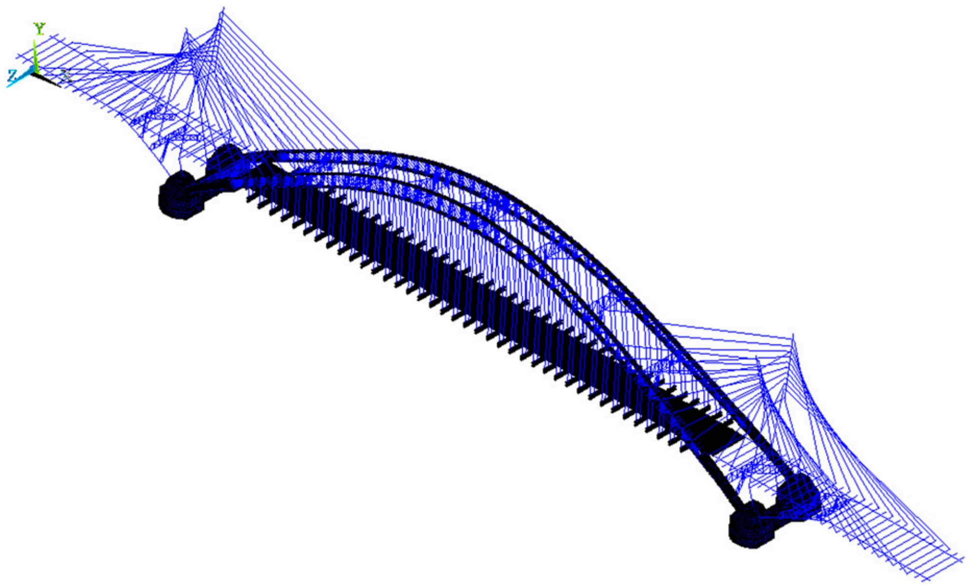

Fig. 2. Finite-element model of the Liancheng Bridge in *ANSYS*

Table 2. First 10 Natural Frequencies of Liancheng Bridge (Data from Luo et al. 2005)

	Frequency (Hz)		
Mode number	This model	Reference	Difference (%)
1	0.238	0.234	1.83
2	0.326	0.347	6.10
3	0.439	0.462	4.90
4	0.482	0.538	10.34
5	0.705	0.702	0.49
6	0.740	0.727	1.84
7	0.778	0.825	5.68
8	0.915	0.898	1.86
9	0.928	0.931	0.34
10	0.985	1.021	3.51

$$[M_v]\{\ddot{d}_v\} + [C_v]\{\dot{d}_v\} + [K_v]\{d_v\} = \{F_G\} + \{F_v\} \tag{1}$$

where $[M_v]$, $[C_v]$, and $[K_v]$ = mass, damping, and stiffness matrices of the vehicle, respectively; $\{d_v\}$ = displacement vector of the vehicle; $\{F_G\}$ = gravity force vector of the vehicle; and $\{F_v\}$ = vector of the wheel-road contact forces acting on the vehicle.

Equation of Motion of the Bridge

The equation of motion for a bridge can be written as follows:

$$[M_b]\{\ddot{d}_b\} + [C_b]\{\dot{d}_b\} + [K_b]\{d_b\} = \{F_b\} \tag{2}$$

where $[M_b]$, $[C_b]$, and $[K_b]$ = mass, damping, and stiffness matrices of the bridge, respectively; $\{d_b\}$ = displacement vector of the bridge; and $\{F_b\}$ = vector of the wheel-road contact forces acting on the bridge.

Road Surface Condition

Road surface condition (RSC) is a very important factor that affects the dynamic responses of both the bridge and vehicles. Usually, a road surface profile is assumed to be a zero-mean stationary Gaussian random process and can be generated through an inverse Fourier transformation based on a power spectral density (PSD) function (Dodds and Robson 1973), such as

$$r(X) = \sum_{k=1}^{N} \sqrt{2\phi(n_k)\Delta n}\cos(2\pi n_k X + \theta_k) \tag{3}$$

where θ_k = random phase angle uniformly distributed from 0 to 2π; $\varphi()$ = PSD function ($\mathrm{m}^3/\mathrm{cycles}/\mathrm{m}$) for the road surface elevation; and n_k = wave number (cycles/m). In the current study, the PSD function adopted by Huang and Wang (1992) was used.

The ISO (1995) proposed a road roughness classification index from A (very good) to H (very poor) according to different values of $\varphi(n_0)$. In this study, the classification of road roughness based on ISO (1995) was used.

Assembling the Vehicle-Bridge Coupled System

Based on the displacement relationship and interaction force relationship at the contact points, the vehicle-bridge coupled system can be established by combining the equations of motion of both the bridge and vehicle as follows:

$$\begin{bmatrix} M_b & \\ & M_v \end{bmatrix}\begin{Bmatrix} \ddot{d}_b \\ \ddot{d}_v \end{Bmatrix} + \begin{bmatrix} C_b + C_{b-b} & C_{b-v} \\ C_{v-b} & C_v \end{bmatrix}\begin{Bmatrix} \dot{d}_b \\ \dot{d}_v \end{Bmatrix} + \begin{bmatrix} K_b + K_{b-b} & K_{b-v} \\ K_{v-b} & K_v \end{bmatrix}\begin{Bmatrix} d_b \\ d_v \end{Bmatrix} = \begin{Bmatrix} F_{b-r} \\ F_{b-r} + F_G \end{Bmatrix} \tag{4}$$

where C_{b-b}, C_{b-v}, C_{v-b}, K_{b-b}, K_{b-v}, K_{v-b}, F_{b-r}, and F_{b-r} are the results of the wheel-road contact forces and are time-dependent terms.

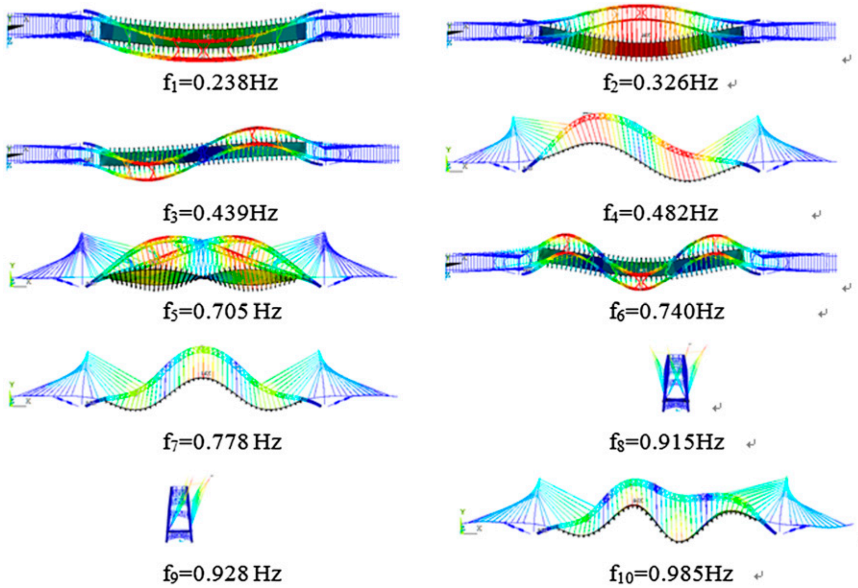

Fig. 3. First 10 mode shapes of Liancheng Bridge in *ANSYS*

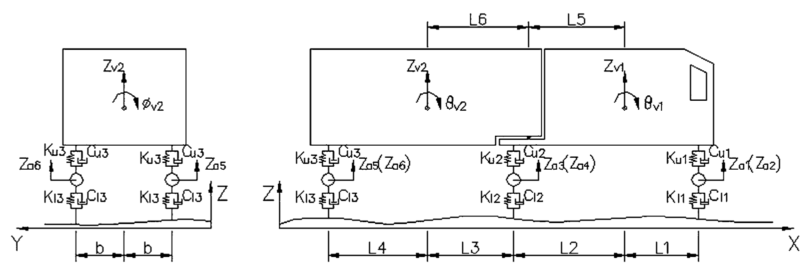

Fig. 4. Analytical model of the HS20-44 truck

To simplify the bridge model and therefore save computational effort, the modal superposition technique can be used, and Eq. (4) can be simplified into the following:

$$\begin{bmatrix} I & \\ & M_v \end{bmatrix}\begin{Bmatrix} \ddot{\xi}_b \\ \ddot{d}_v \end{Bmatrix} + \begin{bmatrix} 2\omega_i\eta_i I + \Phi_b^T C_{b-b}\Phi_b & \Phi_b^T C_{b-v} \\ C_{v-b}\Phi_b & C_v \end{bmatrix}\begin{Bmatrix} \dot{\xi}_b \\ \dot{d}_v \end{Bmatrix} + \begin{bmatrix} \omega_i^2 I + \Phi_b^T K_{b-b}\Phi_b & \Phi_b^T K_{b-v} \\ K_{v-b}\Phi_b & K_v \end{bmatrix}\begin{Bmatrix} \xi_b \\ d_v \end{Bmatrix} = \begin{Bmatrix} \Phi_b^T F_{b-r} \\ F_{b-r} + F_G \end{Bmatrix} \tag{5}$$

The vehicle-bridge coupled system in Eq. (5) contains only the modal properties of the bridge and physical parameters of the vehicles. As a result, the complexity of solving the vehicle-bridge coupling equations is greatly reduced. A *MATLAB 2012b* program was developed to assemble the vehicle-bridge coupled system in Eq. (5) and solve it using the fourth-order Runge-Kutta method in the time domain. The time step was set to 0.01 s to achieve numerical convergence. A sensitivity study was conducted on the effect of the number of modes on the accuracy of the simulation results. A few numbers of modes, including 10, 20, 50, 80, 150, and 200 modes, were studied, and the simulated bridge deflection and strain (both in the vertical and transverse directions) at the midspan of the bridge when the truck travels across the bridge at a speed of 0.5 m/s were compared with the static results obtained from the finite-element analysis in the *ANSYS* program. The use of 200 modes can produce results with satisfactory accuracy, with the maximum difference for all responses falling below 2%. Therefore, the first 200 modes were used in the numerical simulations. For more details of the bridge-vehicle coupled system and solving process, readers can refer to Deng and Cai (2010a, b).

Numerical Simulations

Two important indexes are usually investigated in the study of bridge vibration under the effect of moving vehicles. One is the dynamic IM, which is also referred to as the dynamic load allowance (DLA), and the other is the perceptible level of vibration (Biggs 1964). In addition to these two indexes, the ride comfort for the bridge was also examined. In the following sections, the studies on the dynamic IM, perceptible level of vibration, and ride comfort will be presented, and the results will be discussed.

Dynamic IM

Dynamic analysis of bridges under vehicle loading has been studied extensively in the last 2 decades. A number of parameters affecting the dynamic IM have been studied, including the bridge types,

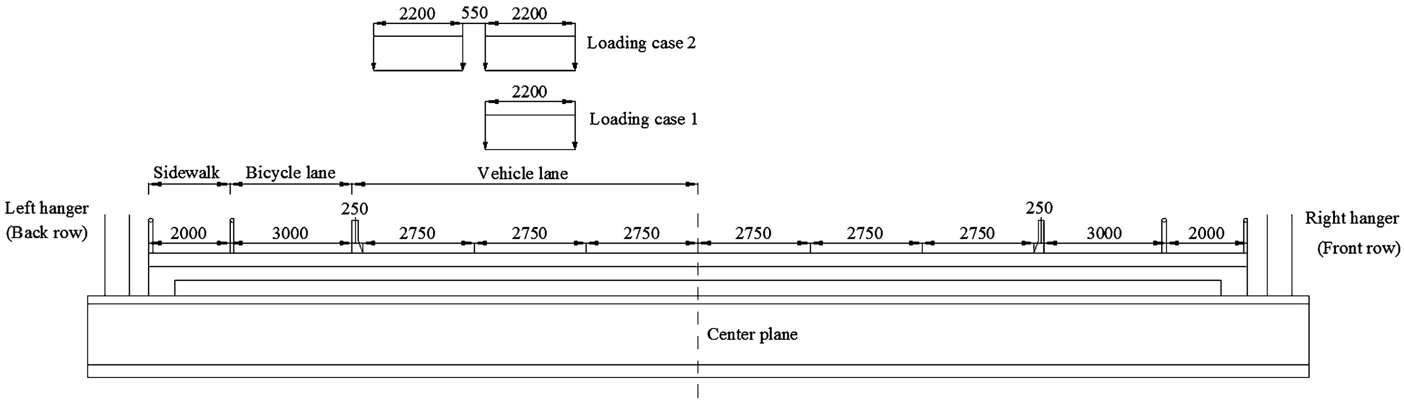

Fig. 5. Two loading cases considered in this study

vehicle loading positions, vehicle properties (including weight, stiffness, damping, etc.), vehicle traveling speeds, number of loading lanes, RSCs, and so forth (Huang et al. 1993; Chang and Lee 1994; Yang et al. 1995; Liu et al. 2002; Deng and Cai 2010a; Beben 2013). In the current study, the effects of three important parameters (i.e., vehicle loading condition, vehicle speed, and RSC) on the dynamic IMs were investigated. The dynamic IMs are defined as

$$\mathrm{IM} = \frac{R_{\mathrm{dyn}} - R_{\mathrm{sta}}}{R_{\mathrm{sta}}} \tag{6}$$

where R_{dyn} and R_{sta} = maximum dynamic and static responses of the target point, respectively.

In the current study, five vehicle speeds ranging from 30 to 110 km/h with intervals of 20 km/h were considered, and three different RSCs were studied according to ISO (1995), namely, good, average, and poor. In this study, the variation of road surface elevation in the transverse direction was not considered. Two loading cases were considered as shown in Fig. 5.

To investigate the relationship between the three parameters and dynamic IM, under each condition with certain combinations of the three parameters (with a given vehicle speed, RSC, and loading case), the vehicle-bridge interaction analysis was set to run 20 times with 20 randomly generated road surface profiles under the given RSC. Then, the average value of the 20 IMs was obtained. Twenty IMs were considered to be enough based on a statistical analysis, which shows that the variation of the estimated mean of the IMs can be controlled within a satisfactory range with 20 IMs considered (Liu et al. 2002; Deng and Cai 2010a, b).

In this study, the dynamic responses of different bridge components were used for studying the dynamic IM, including the main towers, main arch ribs, side span arch ribs, stay cables, hangers, bridge deck and transverse girders, and so forth. Because the bridge is symmetrical about the midspan, only the left half of the bridge, shown in Fig. 1(a), was studied. Similarly, because the bridge structure (back and front rows) is symmetrical about the central vertical plane, only the bridge components on the back row (left part in Fig. 5) were studied.

A total of 10 points (or locations), marked from P_1 to P_{10} in Fig. 1, were first selected as the reference points for the dynamic IM. These points were selected based on two considerations: (1) different types of key structural components should be included; and (2) components/points with the maximum static response among bridge components of the same type should be selected. In addition to these 10 points selected in the back row, two points in the front row (P_{16} and P_{18}) were added to the selection for the purpose of comparison. These two pairs of points (P_6 and P_{16}, P_8 and P_{18}) are symmetrical about the central vertical plane as shown in Fig. 1(b). A description of all the points selected is provided in Table 3.

Table 3. Description of Points Selected and Corresponding Static Bridge Responses

Point number	Position of selected point	Static strain ($\mu\varepsilon$) Loading Case 1	Static strain ($\mu\varepsilon$) Loading Case 2
P_1	Stay cable of left side span with maximum tension	12.96	22.85
P_2	Arch rib of left side span with maximum compression	10.47	22.21
P_3	Left main tower with maximum compression	0.62	1.27
P_4	Left foot of main arch rib	3.82	7.95
P_5	Stay cable (within main span) with maximum tension	26.76	57.27
P_6	Hanger with maximum tension in the back row	132.40	278.40
P_{16}[a]	Hanger with maximum tension in the front row	68.51	117.80
P_7	Center of main arch rib	3.88	8.28
P_8	Center hanger in the back row	102.50	218.20
P_{18}[a]	Center hanger in the front row	50.74	87.15
P_9	Bridge deck at midspan with maximum strain	8.64	18.09
P_{10}	Transverse girder at midspan with maximum strain	1.58	3.22

[a]Selected from the front row of the bridge while all other 10 points (P_1−P_{10}) are selected from the back row of the bridge.

The average IMs obtained from the numerical simulations for three RSCs under two loading cases are plotted against the vehicle speed in Fig. 6, where plots for different points are separated.

As shown in the results in Fig. 6, the dynamic IMs obtained from Loading Case 1 (with one lane loaded) are generally greater than those obtained from Loading Case 2 (with two lanes loaded). This observation is consistent with the findings reported by other researchers (Kim and Nowak 1997; Huang 2005; Ashebo et al. 2007). In many cases, this conclusion can actually be extended to the cases with the same loading condition, in which the dynamic IMs of bridge components bearing a smaller amount of vehicle loads are usually greater than those of bridge components bearing a larger amount of vehicle loads (Laman et al. 1999; Shi 2006; Moghimi and

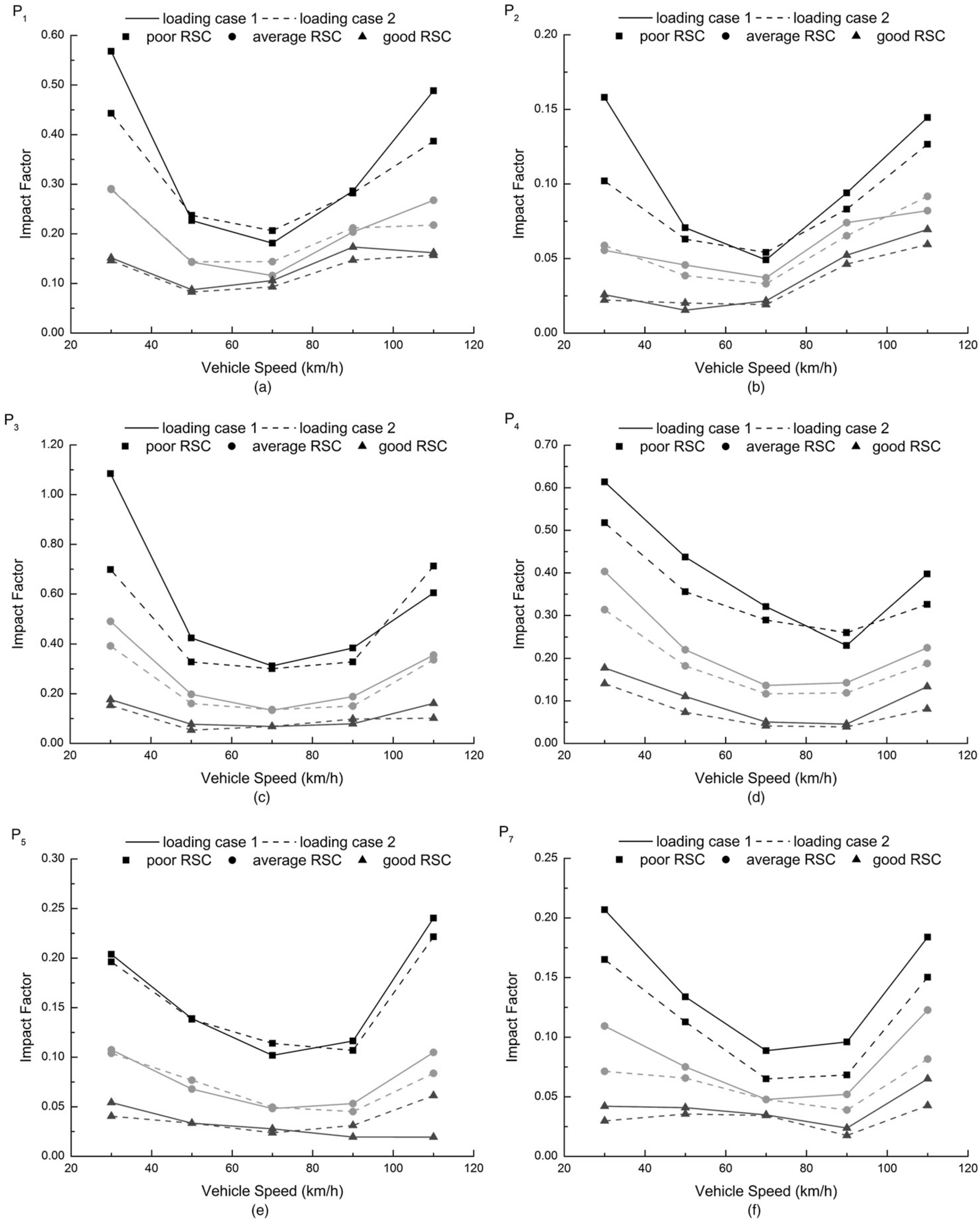

Fig. 6. IMs of studied points: (a) P1; (b) P2; (c) P3; (d) P4; (e) P5; (f) P7; (g) P6; (h) P16; (i) P8; (j) P18; (k) P9; (l) P10

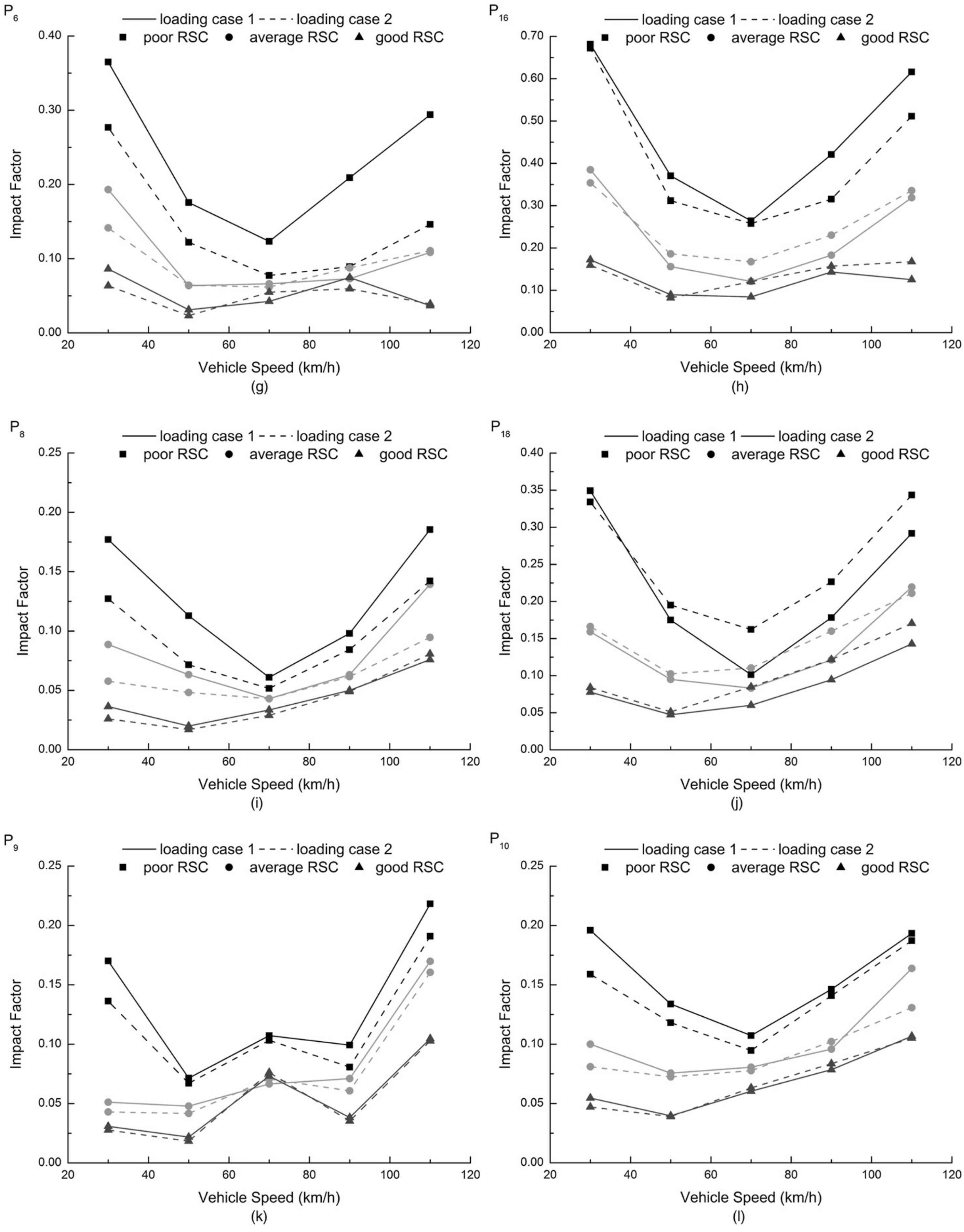

Fig. 6. (*Continued.*)

Ronagh 2008). This also can be confirmed by comparisons of the IMs of the two pairs of points symmetrical about the central vertical plane (P_6 and P_{16}, P_8 and P_{18}).

In Fig. 6, the RSC has a significant impact on the dynamic IMs. The IMs increase significantly as the RSCs become worse. However, the IMs do not necessarily increase with the increase of vehicle speed, which has also been reported by other researchers (Cantieni 1983; Liu et al. 2002; Brady et al. 2006; Deng and Cai 2010a). Interestingly, in this study, the dynamic IMs obtained at a vehicle speed of 30 km/h are almost equivalent to those at a speed of 110 km/h. One possible interpretation may be that the quasi-resonance of the vehicle-bridge system may occur when the truck is moving at a speed of 30 km/h. An in-depth examination shows that the loading frequency of the vehicle at a speed of 30 km/h, provided that the vehicle is simplified as a series of concentrated forces, is 1.953 Hz. According to Shi et al. (2008), when *n* times the loading frequency equals the natural frequency of the bridge, the quasi-resonance will occur. For Liancheng Bridge, the 14th frequency of the bridge (corresponding to a vertical vibration mode with a frequency of 1.959 Hz) is very close to the loading frequency of the vehicle. Therefore, the quasi-resonance is expected to occur, and the IM is amplified. To verify this phenomenon, the strain time histories of the center point of the main arch rib (P_7) at different speeds under the average road roughness condition are provided in Fig. 7. A truck traveling at 30 km/h induces the largest maximum dynamic strain response at point P_7 among all given speeds, indicating that the quasi-resonance is more prone to occur at a speed of 30 km/h than other speeds considered for the case. Also, the dynamic component of the strain at point P_7 decreases when the truck speed increases from 30 to 70 km/h and then increases when the truck speed increases from 70 to 110 km/h. This is consistent with the variation of the IM with vehicle speed obtained from the analysis.

In Fig. 6, the dynamic IMs vary significantly between the different points (or bridge components) analyzed. The IMs of the side span arch rib (P_2), stay cable in the main span (P_5), main arch rib vault (P_7), middle hanger (P_8), bridge deck (P_9) and transverse girder (P_{10}) are all below 0.33, the specified dynamic IM in the AASHTO's *LRFD Bridge Design Specifications* (AASHTO 2004), even under poor RSCs. However, the IMs of the stay cable in the side span (P_1), main tower (P_3), left foot of the main arch rib (P_4), and hanger with maximum tension in the front row (P_6) may exceed 0.33 under poor or even average RSCs. However, the internal forces at these points are generally small. Therefore, these points are not likely to be the critical points for strength design or evaluation of the bridge.

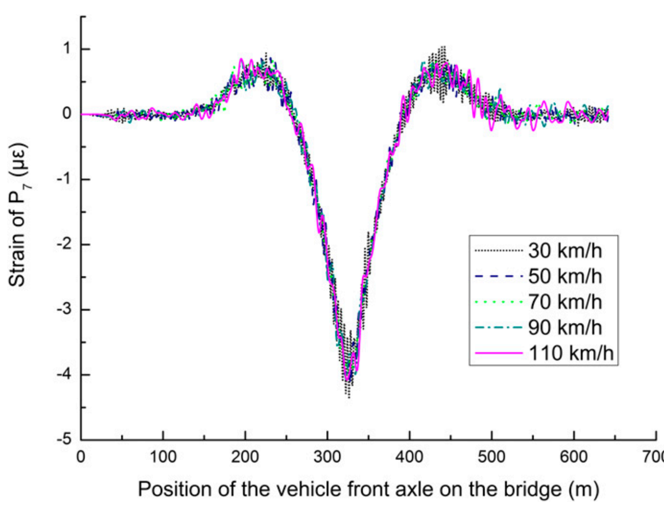

Fig. 7. Strain time histories of the center point of the main arch rib (P_7) at different speeds under the average road roughness condition

Perceptible Level of Bridge Vibration

Much research has been devoted to investigating the perceptible level of vibration of highway bridges, including both experimental studies and numerical simulations (Kobori and Kajikawa 1974; Yoshimura et al. 2006; Moghimi and Ronagh 2008; Rizwan et al. 2013). In most of the previous studies, vibration amplitude, frequency, velocity, and acceleration were used as the parameters for evaluating human perception of bridge vibration. Based on a series of experimental studies, Kobori and Kajikawa (1974) suggested that vertical velocity is the most effective index in evaluating the perception of vibration. In this paper, the vertical velocity of the bridge deck is, therefore, used as the parameter when evaluating the perceptible level of bridge vibration.

Fig. 8 shows the maximum velocities of points along the bridge deck under three different road conditions when the truck(s) moves across the bridge at a speed of 70 km/h. These points were selected from cross sections with an interval of 5 m in the bridge longitudinal direction. At each cross section, the point with the largest vertical

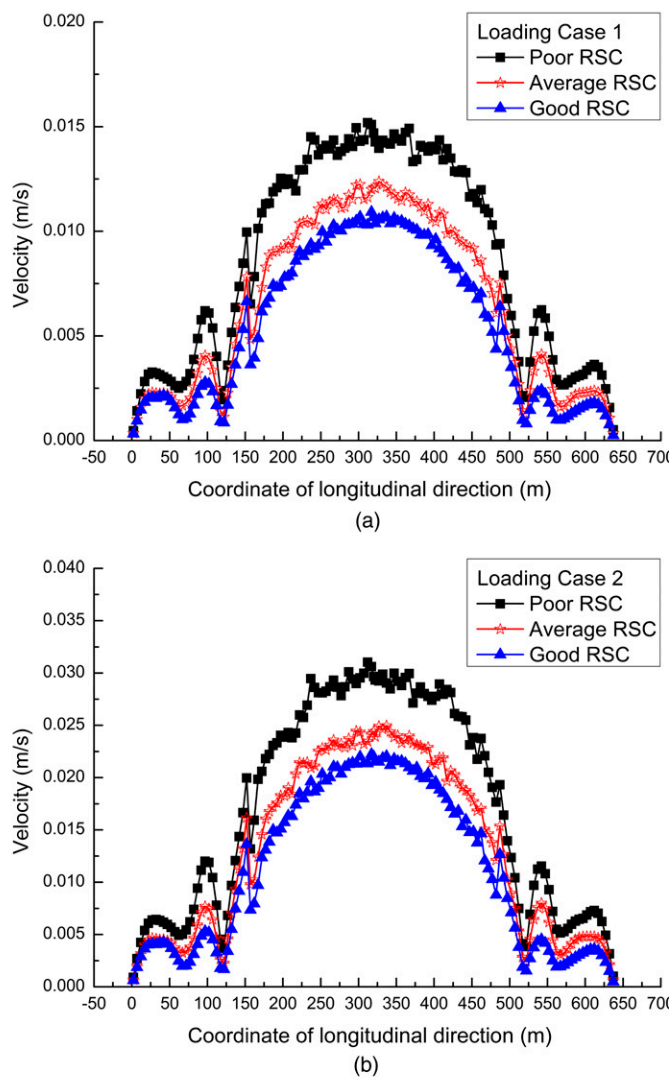

Fig. 8. Maximum velocities of bridge deck when the truck(s) moves across the bridge: (a) Loading Case 1; (b) Loading Case 2

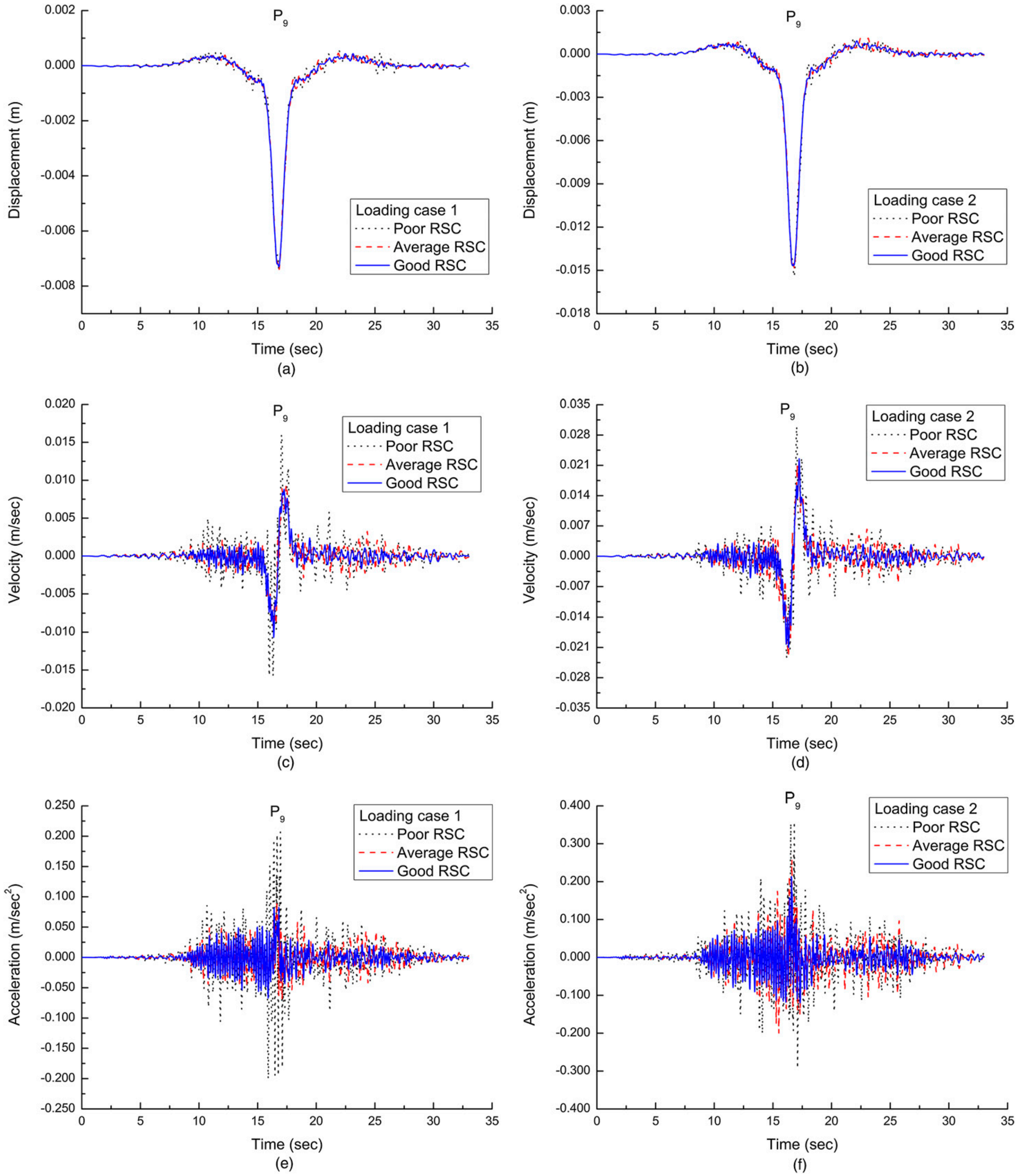

Fig. 9. Response time histories of bridge deck at midspan under the two loading cases: (a) displacement of P9 under Loading Case 1; (b) displacement of P9 under Loading Case 2; (c) velocity of P9 under Loading Case 1; (d) velocity of P9 under Loading Case 2; (e) acceleration of P9 under Loading Case 1; (f) acceleration of P9 under Loading Case 2

displacement was selected. The vertical axis in Fig. 8 represents the maximum velocity obtained from the velocity time history for each selected point during the entire process when the truck(s) moves across the bridge.

Fig. 9 shows the displacement, velocity, and acceleration time histories for the point on the bridge deck at the midspan position (P_9) under the two loading conditions and three different RSCs. As can be seen in Fig. 9, the effect of the RSCs on the largest displacement of point P_9 is insignificant though the dynamic effect increases as the RSC becomes worse. However, the effect of the RSC on velocity and acceleration responses of Point P_9 is significant. Fig. 9 shows that under Loading Case 1, the magnitudes of both velocity and acceleration under poor RSCs are almost twice those under good RSCs. In Fig. 9, when the truck(s) reaches the position of P_9, significant impulse was generated on both the velocity and acceleration responses, causing large local impact on the bridge deck.

Table 4 provides the maximum velocities of the points on the bridge deck from the main span and side span for the two loading cases, respectively. Under the two loading cases, both the maximum velocities of the bridge deck at the main span and side span increase when the RSC deteriorates. The maximum velocities under Loading Case 2 are almost twice the corresponding maximum velocities under Loading Case 1, which may be largely attributed to the linear-elastic assumption adopted for the bridge model because the truck load doubles under Loading Case 2.

The perceptible vibration of the bridge induced by moving vehicles can be evaluated by the ergonomic evaluation method developed by Kobori and Kajikawa (1974). The vibration stimulation, S (cm/s), is calculated according to the effective value of the maximum velocity, V_{max} (cm/s), which can be expressed as follows:

$$S = \frac{V_{\max}}{\sqrt{2}} \tag{7}$$

The vibration greatness level (VGL) (in decibels) can then be determined by the following equations:

$$\mathrm{VGL} = 20\log_{10}(S/S_0) \quad \left(S_0 = 1.4 \times 10^{-2}\ \mathrm{cm/s}\right) \tag{8}$$

$$\log_{10}\mathrm{VG} = 0.05(\mathrm{VGL} - 40) \quad \text{when} \quad \mathrm{VGL} \le 40\ \mathrm{dB} \tag{9}$$

$$\log_{10}\mathrm{VG} = 0.03(\mathrm{VGL} - 40) \quad \text{when} \quad \mathrm{VGL} > 40\ \mathrm{dB} \tag{10}$$

Different perceptible levels and corresponding lower limits of vibration greatness (VG) for pedestrians are provided in Table 5 (Kobori and Kajikawa 1974). The results of maximum velocities, VGLs, and corresponding categories for the Liancheng Bridge under the two loading cases are summarized in Table 6. Both the RSC and loading condition greatly affect the vibration level of the bridge. Under Loading Case 1, the perceptible level switches from slightly perceptible to definitely perceptible when the RSC changes from good to poor. Under Loading Case 2, the perceptible level changes from definitely perceptible to slightly hard to walk when the RSC changes from good to poor.

Table 4. Maximum Velocities of Bridge Deck with Different RSCs and Loading Cases

RSC	Maximum velocity of main span (cm/s)	Maximum velocity of side span (cm/s)
Good	1.09[a]/2.22[b]	0.28/0.53
Average	1.24/2.50	0.41/0.77
Poor	1.52/3.19	0.62/1.20

[a]Loading Case 1.
[b]Loading Case 2.

Table 5. Perceptible Levels and Corresponding Lower Limits of VG for Pedestrians

Perceptible level	VG limit
Slightly perceptible	0.32
Definitely perceptible	0.61
Slightly hard to walk	1.12
Extremely hard to walk	1.48

Ride Comfort of the Bridge

In ISO 2631-1 (ISO 1997), the RMS magnitudes of acceleration are used as the index for ride comfort. The ride comfort levels are defined based on the RMS magnitudes of acceleration as shown in Table 7.

For vibrations in more than one direction, a weighted RMS for acceleration, a_w, is also defined in ISO 2631-1 as a function of vibrations in all three orthogonal directions and is calculated as

$$a_w = \left(k_{aw}^2 a_{wx}^2 + k_{ay}^2 a_{wy}^2 + k_{az}^2 a_{wz}^2\right)^{1/2} \tag{11}$$

where a_{wx}, a_{wy}, and a_{wz} = weighted RMS accelerations with respect to the orthogonal axes x, y, and z, respectively; k_{aw}, k_{ay}, and k_{az} = weighting factors for the orthogonal axes x, y, and z, respectively; and

$$a_{wj}\Big|_{j=x,y,z} = \left(\frac{1}{T}\int_{t=0}^{t=T} a_{wj}^2\Big|_{j=x,y,z} dt\right)^{1/2} \tag{12}$$

where $a_{wj}\big|_{j=x,y,z}$ = acceleration as a function of time (m/s^2) in the x-, y-, and z-directions; and T = duration of the measurement (s) (Yin et al. 2011).

Table 6. Response Level of Liancheng Bridge

Road roughness condition	V_{max} (cm/s)	VG	Perceptible level
Good	1.09[a]/2.22[b]	0.55/1.07	Slightly perceptible/ definitely perceptible
Average	1.24/2.50	0.63/1.15	Definitely perceptible/ slightly hard to walk
Poor	1.52/3.19	0.77/1.33	Definitely perceptible/ slightly hard to walk

[a]Loading Case 1.
[b]Loading Case 2.

Table 7. Ride Comfort Levels Defined in ISO 2631-1

Acceleration magnitudes, a_w (m/s^2)	Comfort level
<0.315	Not uncomfortable
0.315–0.63	A little uncomfortable
0.5–1	Fairly uncomfortable
0.8–1.6	Uncomfortable
1.25–2.5	Very uncomfortable
>2	Extremely uncomfortable

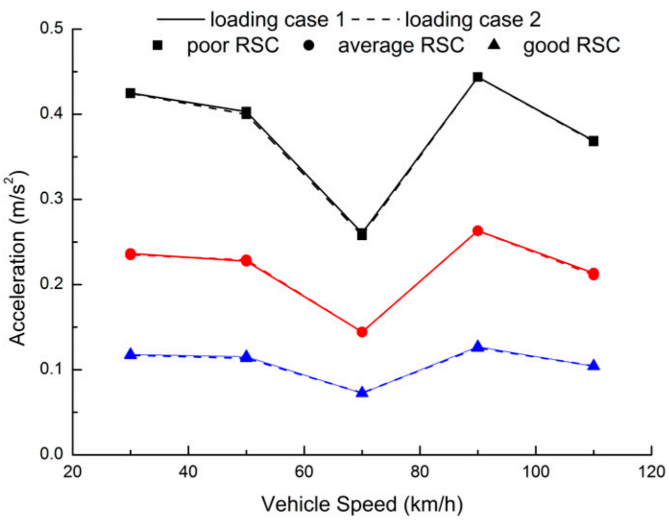

Fig. 10. Vertical acceleration of driver cab

Although that the weighted RMS acceleration consists of accelerations in all three orthogonal directions, in this study the truck is assumed to move along a straight line in the bridge longitudinal direction with a constant speed. Therefore, the weighted RMS acceleration is solely determined by the vertical acceleration.

Fig. 10 plots the maximum vertical acceleration of the driver cab as a function of vehicle speed under the two loading cases and three different RSCs. The following observations can be made from Fig. 10. First, the vertical accelerations of the driver cab obtained from the two different loading conditions are almost equal to each other, indicating that the addition of another running vehicle on the bridge is not likely to affect the comfort level of an existing vehicle. Second, the vertical acceleration of the driver cab does not necessarily increase with the increase of vehicle speed. Third, the RSC has a considerable effect on the vertical acceleration of the driver cab. As the RSC becomes worse, the vertical acceleration of the driver cab becomes larger; consequently, the comfort level declines significantly. For the Liancheng Bridge, the driver may not feel uncomfortable under good or average RSCs, whereas the driver can feel a little uncomfortable when the RSC is poor.

Conclusions

In this paper, the dynamic analysis of a cable-stayed CFST arch bridge, the Liancheng Bridge in China, under vehicle loading, is presented. The dynamic IM, perceptible level of vibration, and ride comfort of the cable-stayed CFST arch bridge are investigated. The effect of the vehicle loading condition, vehicle speed, and RSC is investigated. Based on the results from this study, the following conclusions can be drawn.

1. The calculated IMs vary between different bridge components and locations selected. In general, the IMs of bridge components/locations bearing a greater amount of vehicle loads are usually smaller than those of bridge components/locations bearing a lesser amount of vehicle loads. Dynamic IMs increase significantly as the RSC deteriorates; however, an increase in vehicle speed does not necessarily lead to an increase in dynamic IMs. For Liancheng Bridge, the IMs of the key locations of the main load-carrying components of the bridge are mostly below the 0.33 prescribed by the AASHTO's *LRFD Bridge Design Specifications* (AASHTO 2004), even under poor RSCs.
2. The maximum vertical velocity of the bridge, and therefore the perceptible level of vibration, is greatly affected by the RSC and number of loading lanes. For Liancheng Bridge, under the situation where two trucks drive side by side on a poor road surface, pedestrians can feel it is slightly hard to walk on the bridge.
3. The ride comfort of the driver cab is greatly affected by the RSC. However, the effect of the number of loading lanes on the ride comfort is negligible. In other words, the ride comfort of one vehicle is almost unaffected by another vehicle running on the bridge. For Liancheng Bridge, truck drivers may feel a little uncomfortable when the RSC is poor. However, the comfort level does not necessarily decrease when the vehicle speed increases.

Because all three indexes studied are found to be greatly affected by the RSC, establishing and maintaining a regular program of maintenance is very important to assure both the safety and serviceability of Liancheng Bridge.

Acknowledgments

The authors acknowledge financial support provided by the National Natural Science Foundation of China (Grant No. 51208189) and Excellent Youth Foundation of Hunan Scientific Committee (Grant No. 14JJ1014).

References

AASHTO. (2004). *AASHTO LRFD bridge design specifications*, Washington, DC.

ANSYS 10.0 [Computer software]. Canonsburg, PA, Ansys.

Ashebo, D. B., Chan, T. H. T., and Yu, L. (2007). "Evaluation of dynamic loads on a skew box girder continuous bridge. Part II: Parametric study and dynamic load factor." *Eng. Struct.*, 29(6), 1064–1073.

Beben, D. (2013). "Dynamic amplification factors of corrugated steel plate culverts." *Eng. Struct.*, 46, 193–204.

Biggs, J. (1964). *Introduction to structural dynamics*, McGraw Hill, New York.

Brady, S. P., O'Brien, E. J., and Žnidarič, A. (2006). "Effect of vehicle velocity on the dynamic amplification of a vehicle crossing a simply supported bridge." *J. Bridge Eng.*, 10.1061/(ASCE)1084-0702(2006)11:2(241), 241–249.

Cantieni, R. (1983). "Dynamic load tests of highway bridges in Switzerland: 60 years of experience of EMPA." *Research Rep. 271*, Swiss Federal Laboratories for Testing of Materials, Sankt Gallen, Switzerland.

Chang, D., and Lee, H. (1994). "Impact factors for simple-span highway girder bridges." *J. Struct. Eng.*, 10.1061/(ASCE)0733-9445(1994)120:3(704), 704–715.

Deng, L., and Cai, C. S. (2010a). "Development of dynamic impact factor for performance evaluation of existing multi-girder concrete bridges." *Eng. Struct.*, 32(1), 21–31.

Deng, L., and Cai, C. S. (2010b). "Identification of dynamic vehicular axle loads: Theory and simulations." *J. Vib. Control*, 16(14), 2167–2194.

Dodds, C. J., and Robson, J. D. (1973). "The description of road surface roughness." *J. Sound Vib.*, 31(2), 175–183.

Han, L., Tao, Z., and Liu, W. (2001). "Concrete filled steel tubular structures from theory to practice." *J. Fuzhou Univ.*, 29(6), 24–33.

Huang, D. (2005). "Dynamic and impact behavior of half-through arch bridges." *J. Bridge Eng.*, 10.1061/(ASCE)1084-0702(2005)10:2(133), 133–141.

Huang, D., and Wang, T.-L. (1992). "Impact analysis of cable-stayed bridges." *Comput. Struct.*, 43(5), 897–908.

Huang, D., Wang, T.-L., and Shahawy, M. (1993). "Impact studies of multigirder concrete bridges." *J. Struct. Eng.*, 10.1061/(ASCE)0733-9445(1993)119:8(2387), 2387–2402.

ISO. (1995). “Mechanical vibration-road surface profiles—Reporting of measured data.” *ISO 8068*, Geneva.
ISO. (1997). “Mechanical vibration and shock—Evaluation of human exposure to whole body vibration—Part 1: General requirements.” *ISO 2631-1*, Geneva.
Kang, H. J., Zhao, Y. Y., Zhu, H. P., and Jin, Y. X. (2013). “Static behavior of a new type of cable-arch bridge.” *J. Constr. Steel Res.*, 81, 1–10.
Kim, S., and Nowak, A. S. (1997). “Load distribution and impact factors for I-girder bridges.” *J. Bridge Eng.*, 10.1061/(ASCE)1084-0702(1997)2:3(97), 97–104.
Klein, P., and Yamout, M. (2003). “Cable-stayed arch bridges, Putrajaya, Kuala Lumpur, Malaysia.” *Struct. Eng. Int.*, 13(3), 196–199.
Kobori, T., and Kajikawa, Y. (1974). “Ergonomic evaluation methods for bridge vibrations.” *J. Struct. Mech. Earthq. Eng.*, 230, 23–31 (in Japanese).
Laman, J. A., Pechar, J. S., and Boothby, T. E. (1999). “Dynamic load allowance for through-truss bridges.” *J. Bridge Eng.*, 10.1061/(ASCE)1084-0702(1999)4:4(231), 231–241.
Liu, C., Huang, D., and Wang, T.-L. (2002). “Analytical dynamic impact study based on correlated road roughness.” *Comput. Struct.*, 80(20–21), 1639–1650.
Luo, S., Wang, X., Wang, T., and Gui, X. (2005). “Considerations and study of innovative techniques for long-span cable-stayed arch bridge.” *Bridge Constr.*, 6, 31–33 (in Chinese).
MATLAB 2012b [Computer software]. Natick, MA, MathWorks.
Moghimi, H., and Ronagh, H. R. (2008). “Impact factors for a composite steel bridge using non-linear dynamic simulation.” *Int. J. Impact Eng.*, 35(11), 1228–1243.
Nakamura, S., Tanaka, H., and Kato, K. (2009). “Static analysis of cable-stayed bridge with CFT arch ribs.” *J. Constr. Steel Res.*, 65(4), 776–783.
Rizwan, S. A., Qureshi, M. A., and Najam, F. A. (2013). “In-situ health assessment of poorly executed pre-stressed in-service concrete bridge and suggesting a rehabilitation strategy—A case study.” *Procedia Eng.*, 54, 636–647.
Shi, X. (2006). “Structural performance of approach slab and its effect on vehicle induced bridge dynamic response.” Ph.D. dissertation, Dept. of Civil and Environmental Engineering, Louisiana State Univ., Baton Rouge, LA.
Shi, X., Cai, C. S., and Chen, S. (2008). “Vehicle induced dynamic behavior of short-span slab bridges considering effect of approach slab condition.” *J. Bridge Eng.*, 10.1061/(ASCE)1084-0702(2008)13:1(83), 83–92.
Wu, Q., Takahashi, K., Chen, B., and Nakamura, S. (2006). “Study on dynamic properties of a concrete filled tubular (CFT) arch bridge constructed in China.” *Rep. Faculty Eng. Nagasaki Univ.*, 36(67), 32–39.
Yang, Y.-B., Liao, S.-S., and Lin, B.-H. (1995). “Impact formulas for vehicles moving over simple and continuous beams.” *J. Struct. Eng.*, 10.1061/(ASCE)0733-9445(1995)121:11(1644), 1644–1650.
Yin, X., Fang, Z., and Cai, C. S. (2011). “Lateral vibration of high-pier bridges under moving vehicular loads.” *J. Bridge Eng.*, 10.1061/(ASCE)BE.1943-5592.0000170, 400–412.
Yoshimura, M., Wu, Q. X., Takahashi, K., Nakamura, S., and Furukawa, K. (2006). “Vibration analysis of the Second Saikai Bridge—A concrete filled tubular (CFT) arch bridge.” *J. Sound Vib.*, 290(1–2), 388–409.
Zhao, Y. Y., Yang, X. Z., and Kang, H. J. (2005). “Analysis of dynamic characteristics for cable-stayed arch bridge.” *Highway*, 11, 36–40 (in Chinese).